J Shoulder Elbow Surg (2015) 24, 1789-1800

ELSEVIER

Journal of Shoulder and Elbow Surgery

www.elsevier.com/locate/ymse

# Assessment of glenoid chondral healing: comparison of microfracture to autologous matrix-induced chondrogenesis in a novel rabbit shoulder model

**Vincent M. Wang, PhD[a], Vasili Karas, MS, MD[a], Andrew S. Lee, MS, MD[a], Ziying Yin, PhD[b], Geoffrey S. Van Thiel, MD, MBA[c], Kristen Hussey, MA[a], D. Rick Sumner, PhD[d], Susan Chubinskaya, PhD[e], Richard L. Magin, PhD[b], Nikhil N. Verma, MD[a], Anthony A. Romeo, MD[a], Brian J. Cole, MD, MBA[a,*]**

[a]*Department of Orthopedic Surgery, Rush University Medical Center, Chicago, IL, USA*
[b]*Department of Bioengineering, University of Illinois at Chicago, Chicago, IL, USA*
[c]*Rockford Orthopedic Associates, Rockford, IL, USA*
[d]*Department of Anatomy and Cell Biology, Rush University Medical Center, Chicago, IL, USA*
[e]*Department of Biochemistry, Rush University Medical Center, Chicago, IL, USA*

**Background:** Management of glenohumeral arthrosis in young patients is a considerable challenge, with a growing need for non-arthroplasty alternatives. The objectives of this study were to develop an animal model to study glenoid cartilage repair and to compare surgical repair strategies to promote glenoid chondral healing.

**Methods:** Forty-five rabbits underwent unilateral removal of the entire glenoid articular surface and were divided into 3 groups—untreated defect (UD), microfracture (MFx), and MFx plus type I/III collagen scaffold (autologous matrix-induced chondrogenesis [AMIC])—for the evaluation of healing at 8 weeks (12 rabbits) and 32 weeks (33 rabbits) after injury. Contralateral shoulders served as unoperated controls. Tissue assessments included 11.7-T magnetic resonance imaging (long-term healing group only), equilibrium partitioning of an ionic contrast agent via micro–computed tomography (EPIC-μCT), and histologic investigation (grades on International Cartilage Repair Society II scoring system).

**Results:** At 8 weeks, x-ray attenuation, thickness, and volume did not differ by treatment group. At 32 weeks, the T2 index (ratio of T2 values of healing to intact glenoids) was significantly lower for the MFx group relative to the AMIC group ($P = .01$) whereas the T1ρ index was significantly lower for AMIC relative to MFx ($P = .01$). The micro–computed tomography–derived repair tissue volume was significantly higher for MFx than for UD. Histologic investigation generally suggested inferior healing in the AMIC and UD groups relative to the MFx group, which exhibited improvements in both integration of repair tissue with subchondral bone and tidemark formation over time.

The procedures in this study were performed under Institutional Animal Care and Use Committee approval.

*Reprint requests: Brian J. Cole, MD, MBA, 1611 W Harrison St, Suite 300, Chicago, IL 60612, USA.
E-mail address: bcole@rushortho.com (B.J. Cole).

1058-2746/$ - see front matter 
http://dx.doi.org/10.1016/j.jse.2015.06.008

**Discussion:** Improvements conferred by AMIC were limited to magnetic resonance imaging outcomes, whereas MFx appeared to promote increased fibrous tissue deposition via micro–computed tomography and more hyaline-like repair histologically. The findings from this novel model suggest that MFx promotes biologic resurfacing of full-thickness glenoid articular injury.

**Level of evidence:** Basic Science Study, In Vivo Animal Model.



**Keywords:** Glenohumeral; articular cartilage; microfracture; autologous matrix-induced chondrogenesis; animal model

Management of glenohumeral arthrosis in a young patient population is a considerable challenge. In active patients with increased longevity, there is a need for non-arthroplasty alternatives to reliably reduce pain and improve function,[10] primarily because of concerns related to glenoid implant loosening.[41,47] Unfortunately, alternative strategies such as biologic resurfacing procedures (eg, using lateral meniscus or dermal allografts) and glenoid osteochondral grafting result in unacceptably high rates of failure.[22,49] However, bone marrow–stimulating procedures such as microfracture (MFx)[12,36] and concentric reaming of the glenoid[7] have shown promising short-term and midterm results.

A variety of reparative treatment strategies have been developed for the management of focal articular cartilage defects, with most investigations to date focusing on the knee. Although MFx remains a commonly performed procedure,[48] more recent techniques incorporate synthetic and biologic scaffolds (with or without implanted cells) to facilitate the organized adhesion, migration, and differentiation of mesenchymal stem cells to chondrocytes, thereby facilitating cartilage regeneration.[9,14] One such approach, autologous matrix-induced chondrogenesis (AMIC), is a single-step procedure combining MFx and a type I/III (bilayer) collagen patch, and it has yielded promising results in both preclinical and retrospective clinical studies.[11,16,17,51]

Presently, very little is known regarding the reparative capacity of injured glenohumeral joint (GHJ) articular cartilage. Although numerous animal models across multiple species have been developed for detailed investigation of knee cartilage repair strategies,[6] very few models exist for reliable assessment of glenohumeral chondral injuries (eg, defect models). Therefore, the objectives of this study were to develop an in vivo rabbit model and to compare surgical repair strategies to promote glenoid chondral healing. We hypothesized that both the MFx- and AMIC-treated glenoids would exhibit a superior repair response when compared with untreated defects (UDs).

## Materials and methods

### Experimental design

A total of 45 male New Zealand white rabbits (weighing 4-5 kg at the time of surgery) were randomized into 3 experimental groups and underwent unilateral shoulder surgery. Full-thickness cartilage defects of the entire glenoid were created on the left shoulder and immediately treated with MFx alone, treated with MFx augmented with a collagen scaffold (AMIC), or left as UDs. Contralateral shoulders served as intact controls. Twelve rabbits (4 rabbits per group) were euthanized 8 weeks after surgery for equilibrium partitioning of an ionic contrast agent via micro–computed tomography (EPIC-μCT) followed by histologic analyses, whereas the remaining 33 rabbits (11 rabbits per group) were euthanized at a mean of 32 weeks after surgery for magnetic resonance imaging (MRI), micro–computed tomography (EPIC-μCT), and histologic investigation (Fig. 1). Because of the need for preparation of cored, cylindrical specimens for EPIC-μCT assessment, which rendered the peripheral glenoid tissue unusable, the initial 15 rabbits (5 rabbits per group) in the long-term study were assigned to the histologic study only, thus allowing us to examine the morphology of the entire glenoid articular surface.

### Surgical injury model

The reader is referred to prior studies detailing the anatomy of the rabbit rotator cuff and GHJ.[21,27,54] Under isoflurane anesthesia and by use of a posterolateral approach, a 6-cm craniolateral incision was made on the dorsum of the left shoulder, superior and medial to the GHJ (Fig. 2, *A* and *B*). Skin and soft tissue were dissected down to the junction of the cervical and thoracic trapezius, whose fibers ran perpendicular to the initial incision. The trapezius was reflected along its fibers. The deltoid was then split longitudinally and tagged on both ends to expose the rotator cuff tendons (Fig. 2, *C* and *D*). Next, the supraspinatus tendon was transected transversely at the midline between its musculotendinous junction and its insertion on the humeral head. The supraspinatus was then reflected medially and tagged with a suture. The infraspinatus tendon was similarly incised and reflected medially to expose the joint capsule, which was incised anteriorly. A custom-designed Fukuda-type retractor (Fig. 2, *E*) was used to retract the humeral head posteriorly, providing adequate access to the glenoid in addition to protecting the humeral head cartilage. To create the cartilage defect, a 4-mm arthroscopic burr was used to ream the entire glenoid cartilage surface down to the calcified cartilage layer (Fig. 3, *A*). To avoid mechanically or thermally compromising the humeral cartilage or the surrounding soft-tissue envelope, we performed burring at low speeds and under copious saline solution irrigation. These steps constituted creation of the UD.

Subsequently, in animals assigned to the MFx or AMIC group, 10 MFx holes were created in the subchondral bone with a high-speed 0.7-mm drill to promote bleeding and ingress of bone marrow products (Fig. 3, *B*). The lesion was then irrigated with

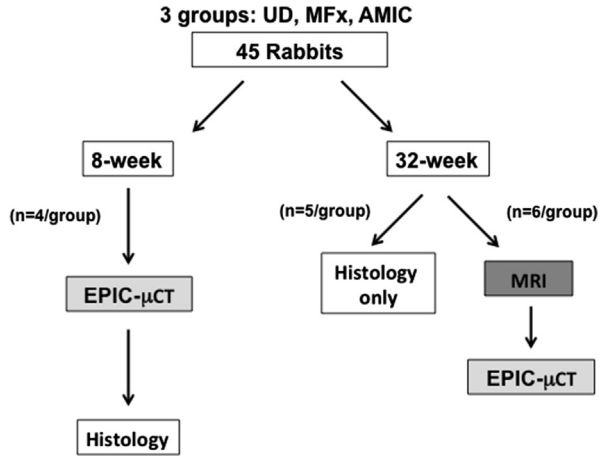


**Figure 1** Experimental design featuring 3 experimental groups: untreated defect (UD), microfracture (MFx), and microfracture with autologous matrix-induced chondrogenesis (AMIC). Left glenoids underwent surgery, whereas right glenoids served as unoperated controls. EPIC-μCT, equilibrium partitioning of an ionic contrast agent via micro–computed tomography; MRI, magnetic resonance imaging.

saline solution, clearing all debris from the joint. For animals assigned to the AMIC group, a type I/III collagen patch (porcine matrix, Bio-Gide; Geistlich Pharma AG, Wolhusen, Switzerland) was then cut to the appropriate size to cover the entirety of the glenoid surface (ie, approximately 7 mm in diameter). As previously described,[2] the bilayer patch (featuring 1 occlusive and 1 porous surface) was oriented such that its porous layer faced the bone. By use of 3 No. 6-0 Vicryl sutures (Ethicon, Somerville, NJ, USA) passed through the scaffold periphery, the patch was secured to the glenoid (Fig. 3, *C*); 2 mattress suture limbs were passed through 2 transosseous tunnels superoanteriorly and superoposteriorly, whereas a third suture limb was secured to the soft tissue inferiorly. The joint space was then irrigated with saline solution, and the humeral head was reduced; the capsule was left unrepaired. The severed ends of the infraspinatus and supraspinatus tendons were reapproximated with No. 4-0 Vicryl sutures. The deltoid and trapezius were also reapproximated and closed with No. 4-0 Vicryl. The skin was then closed with No. 4-0 Monocryl (Ethicon) in a subcuticular fashion.

Postoperatively, the surgical forelimb was immobilized against the body in adduction in neutral flexion using a Velpeau sling for a duration of 1 week to facilitate soft-tissue healing and confer additional stability to the shoulder. The rabbits were housed in individual cages with no further limitations on their motion. Before the fourth postoperative week, all rabbits were able to ambulate without a noticeable limp and none exhibited discernible gait abnormalities.

## Tissue assessments

For the 8-week healing study, glenoid specimens were immersed in 10% neutral buffered formalin (Sigma, St Louis, MO, USA) for 72 hours and stored at room temperature before μCT scanning. For the 32-week healing study, specimens were placed in phosphate-buffered saline solution with protease inhibitors for approximately 1 hour prior to MRI.

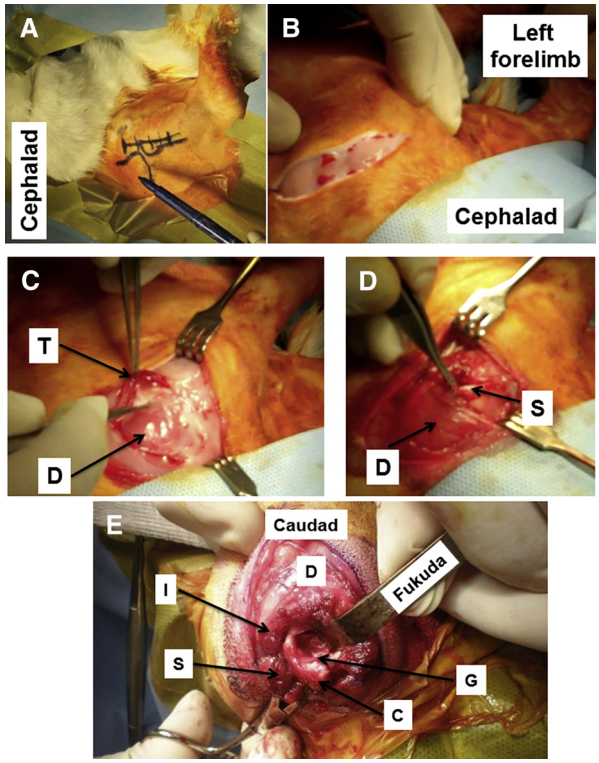


**Figure 2** Surgical approach to rabbit glenohumeral joint. (**A**) Intraoperative preparation of rabbit shoulder. (**B**) Initial incision over the dorsum of a left shoulder through the skin and subcutaneous tissue to the level of the trapezius. (**C**) Dissection through the fibers of the trapezius (T) (reflected by forceps) for exposure of the deltoid (D). (**D**) After a longitudinal split of the deltoid (D) along its fibers, the supraspinatus tendon (S) is identified and transected transversely. The supraspinatus is shown held with forceps. (**E**) After supraspinatus (S) and infraspinatus (I) transection, a custom-designed Fukuda-type retractor is used to retract the humeral head inferiorly and posteriorly to gain access to the glenoid articular surface (G). The coracoid (C) is a useful intraoperative bony landmark. D, deltoid.

## High-field MRI (long-term healing rabbits only)

T2 and T1ρ relaxation times were analyzed in this study because these parameters reflect tissue water content and viscosity and hence characterize, respectively, collagen organization and proteoglycan content of both articular cartilage and chondral repair tissue.[43] Specifically, both free water and water molecules bound to collagen fibers contribute to T2 relaxation,[35,38] whereas proton exchange between water molecules and NH and OH groups in proteoglycans has been suggested as an important contributor to T1ρ relaxation.[1,8,35,38]

From both operated and contralateral intact joints, glenoid plugs (6 mm in diameter) including subchondral bone were harvested immediately after death. In each imaging session, contralateral plugs from 2 rabbits were scanned. Tissue samples were placed in a 10–mm–outer diameter glass nuclear magnetic resonance (NMR) tube filled with Fluorinert (FC-43; 3M, St Paul, MN, USA) to prevent dehydration and to reduce magnetic susceptibility artifacts. Left and right plugs from each animal were

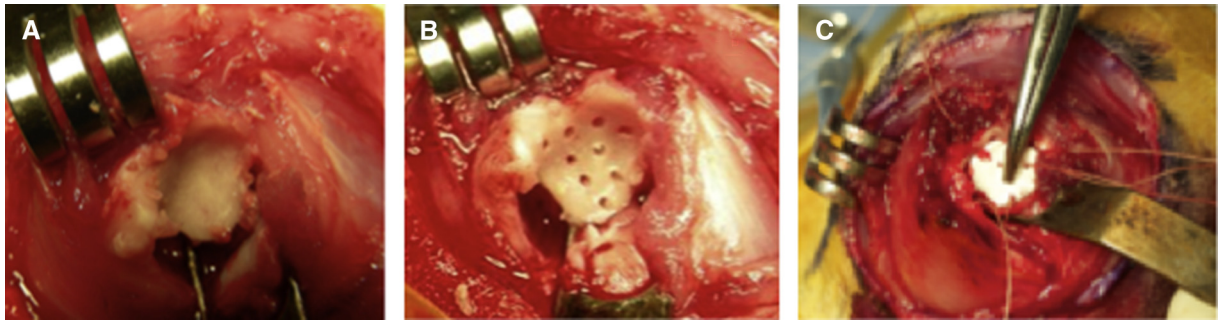


**Figure 3** (**A**) Creation of surgical glenoid defect. (**B**) Creation of microfracture holes (0.7 mm in diameter) after surgical defect creation. (**C**) Autologous matrix-induced chondrogenesis treatment consisting of placement of type I/III bilayer collagen matrix over defect after microfracture.

positioned such that their articular surfaces opposed one another and with the articular surfaces oriented parallel to the main magnetic field ($B_0$). The imaging plane was oriented perpendicular to the static magnetic field to maximize T2 contrast due to the magic angle effect.[4] Experiments were performed using a Bruker DRX 11.7-T Avance spectrometer (54-mm-diameter vertical bore magnet) with a micro-imaging gradient insert (maximum gradient strength of 2,000 mT/m [millitesla per meter]) and a 10-mm radiofrequency (RF) saddle coil (Bruker BioSpin, Billerica, MA, USA).[39,42] High-resolution (62.5 μm × 62.5 μm × 200 μm) proton density–weighted images were acquired using a fast spin-echo pulse sequence with the following imaging parameters: repetition time (TR), 4,000 milliseconds; echo time (TE), 8 milliseconds; matrix size, 128 × 128; field of view, 8 mm × 8 mm; 20 slices; slice thickness, 200 μm; and number of averages, 6. T1ρ relaxation time was measured using a preparatory self-compensation pulse cluster followed by a fast spin-echo sequence[5] with the following acquisition parameters: TE/TR, 8 milliseconds/3,000 milliseconds; spin-lock duration, 10, 20, 40, 80, and 160 milliseconds; spin-lock strength, 100 μT (microtesla); 1 slice; and slice thickness, 500 μm. T2 relaxation time was acquired using a modified CPMG (Carr-Purcell-Meiboom-Gill) sequence[25] with the following acquisition parameters: TR, 10,000 milliseconds; TE, 6.2 to 100 milliseconds; 16 echoes evenly spaced; 6 slices; and slice thickness, 500 μm.

By use of a custom-written MATLAB (The MathWorks, MA, USA) code, the subchondral bone was distinguished from cartilaginous or fibrocartilaginous tissue by adjusting the contrast threshold of proton density–weighted images on the basis of the histogram distribution of signal intensities; contours were then drawn semiautomatically to identify the full-thickness repair or native tissue (or both) in each slice. Tissue volume was computed as the product of the total number of voxels, in-plane X-resolution (62.5 μm), in-plane Y-resolution (62.5 μm), and slice thickness (200 μm). The volume fill ratio was calculated for each sample as the volume of repair tissue (left glenoid) divided by that of the contralateral glenoid.

T1ρ and T2 maps were created using a non-negative least-squares monoexponential fit on a pixel-by-pixel basis. The mean T2 and T1ρ values for each sample were obtained directly from the calculated parametric maps based on a voxel-wise average over the available slice or slices. For each rabbit, a T1ρ index and a T2 index (defined as the ratio of the mean values of the left and right glenoids) were then calculated to standardize the relative T1ρ and T2 changes.[24,45]

The native cartilage (right glenoid) or repair tissue (left glenoid) was further divided into superficial and deep regions (of approximately equal thickness) using a semiautomated approach similar to that described by Theologis et al.[50] In the UD group, reliable quantification of relaxation times was not possible because of the minimal amount of repair tissue consistently observed. The full-thickness T2 and T1ρ values, as well as the T2 and T1ρ indexes, were statistically compared between the MFx and AMIC groups. Deep and superficial T1ρ and T2 values from each sample were compared using a paired comparison. The appropriate statistical test (eg, 2-tailed, paired *t* test or Wilcoxon signed rank test) was selected after assessment of data normality (SPSS software, version 22; IBM, Armonk, NY, USA). Significance was assumed for $P < .05$.

## EPIC-μCT

By use of a previously described technique based on x-ray attenuation properties,[28,40] repair tissue or native cartilage attenuation, thickness, and volume were computed for each glenoid. The EPIC-μCT technique has been shown to be an effective, high-resolution assay for morphologic analysis of cartilage injury in vivo[28] and in vitro.[40,55,56] In this approach, x-ray attenuation patterns can be reliably quantified and mapped spatially as an index of sulfated glycosaminoglycan content within the tissue.[40] Following the methodology previously developed at our institution,[28] formalin-fixed glenoids were incubated in a solution of Ioxaglate (Hexabrix; Mallinckrodt, St Louis, MO, USA) with phosphate-buffered saline solution plus protease inhibitors (Ioxaglate concentration of 40%) in a covered glass centrifuge tube sealed with Parafilm at 37°C for 2 hours and then scanned using a SCANCO μCT 40 scanner (SCANCO Medical AG, Brüttisellen, Switzerland) with a 20-μm resolution in all 3 spatial planes. Pilot studies in our laboratory showed no significant difference in attenuation, average thickness, and average volume between fresh and fixed cartilage samples.

Glenoid specimens were positioned within a 20-mm-diameter plexiglas μCT holder, and scans were carried out at 45 kV (peak), 177 μA, and 300 milliseconds' integration time. After scanning (mean, 412 slices), the specimens were placed in formalin to desorb Hexabrix from the cartilage, after which the formalin was freshly replaced before histologic processing. Image processing and determination of attenuation values were carried out as described by Kotwal et al.[28] In brief, images were manually

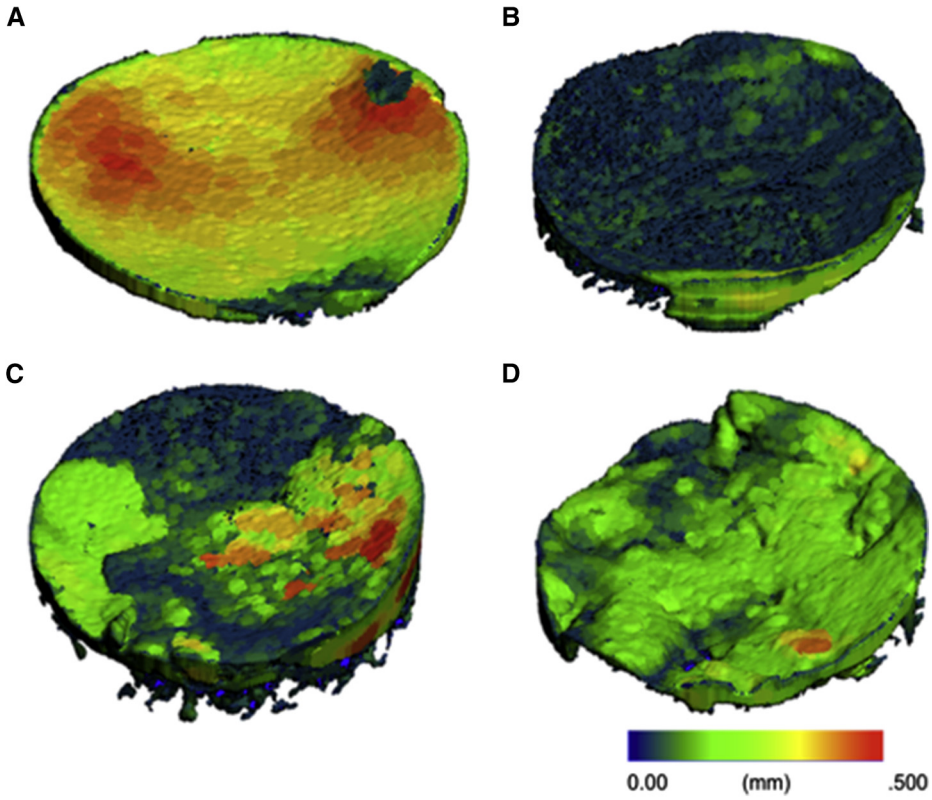


**Figure 4** Representative EPIC-μCT (equilibrium partitioning of an ionic contrast agent via micro–computed tomography)–derived thickness maps for (**A**) intact, (**B**) untreated defect, (**C**) microfracture, and (**D**) autologous matrix-induced chondrogenesis groups 8 weeks after injury.

contoured every 8 to 10 slices to isolate a 5-mm-diameter region of interest containing subchondral bone, cartilage, and air. Intervening slices were contoured using the morphing function of the scanner software, and histograms of the attenuation values were obtained across all slices of the region of interest. Global upper and lower thresholds were selected for cartilage segmentation to measure thickness and volume using the distance transformation function of the scanner software.[23] To assess reproducibility, repeated scans of 8 individual samples were performed, including 2 each from the intact, UD, MFx, and AMIC groups. The coefficients of variation for attenuation, thickness, and volume across groups ranged from 2.0% to 13.4%, which was similar to that obtained for mouse knee joints in our laboratory.[28] Repair-site filling was quantified as the volumetric ratio of repair tissue (left glenoid) to unoperated cartilage (right glenoid). Data were analyzed statistically for comparison of treatment groups and contralateral glenoids within each group following the approach described earlier for MRI results.

### Histologic investigation

Samples were decalcified in EDTA (Bio-Rad Laboratories, Hercules, CA, USA) and embedded in paraffin, and 6-μm sections were generated and stained with either hematoxylin-eosin or safranin O/fast green. Safranin O–stained sections were graded by 2 blinded, independent observers (S.C. and Lev Rappoport, MD), using the International Cartilage Repair Society (ICRS) II guidelines.[33] The ICRS II scoring system includes 14 parameters for the assessment of cellularity, regional cartilage/fibrocartilage and bone tissue structure, inflammation, vascularity, and mineralization; each parameter is scored on a 0 to 100 scale (where 100 indicates normal cartilage features), and the summation of subscores yields a total score per sample. The total ICRS score was averaged from the 2 observers for each sample and statistically compared across groups, as well as between the 2 postoperative time points for each treatment group.

## Results

No significant differences ($P > .45$) in the percentage of weight gain were observed among groups at the time of death of the animals at either time point. On tissue harvest after euthanasia, all GHJs were noted to have stable articulations with no evidence of infection. Collagen scaffold remnants were rarely distinguishable on dissection, implying that the scaffold was successfully integrated into the repair tissue or was completely resorbed by 8 weeks.

## 8-Week healing

### EPIC-μCT

Representative thickness maps are provided in Figure 4. No significant differences in attenuation ($P = .46$), thickness

**Table I** EPIC-μCT results for rabbits 8 weeks and 32 weeks after injury

| | Attenuation | | Thickness, mm | | Volume, $mm^3$ | |
|---|---|---|---|---|---|---|
| | Left | Right | Left | Right | Left | Right |
| 8 wk | | | | | | |
| Untreated | 190 ± 11 | 180 ± 12 | 0.13 ± 0.04 | 0.39 ± 0.01* | 2.82 ± 0.91 | 8.11 ± 0.21* |
| MFx | 190 ± 8* | 181 ± 6 | 0.22 ± 0.08 | 0.34 ± 0.06 | 6.02 ± 2.16 | 7.02 ± 1.18 |
| AMIC | 198 ± 4* | 187 ± 9 | 0.19 ± 0.06 | 0.36 ± 0.05* | 5.12 ± 1.99 | 7.68 ± 0.72 |
| *P* value for 8 wk | .46 | | .28 | | .11 | |
| 32 wk | | | | | | |
| Untreated | 214 ± 20* | 178 ± 45 | 0.10 ± 0.13 | 0.23 ± 0.06* | 1.41 ± 1.40 | 6.44 ± 2.31* |
| MFx | 206 ± 15* | 180 ± 8 | 0.16 ± 0.06 | 0.27 ± 0.04* | 5.55 ± 2.12 | 8.40 ± 2.70 |
| AMIC | 237 ± 27* | 183 ± 13 | 0.20 ± 0.15 | 0.23 ± 0.07 | 4.38 ± 2.41 | 6.92 ± 1.95* |
| *P* value for 32 wk | .13 | | .14 | | .01 | |

*AMIC*, autologous matrix-induced chondrogenesis; *EPIC-μCT*, equilibrium partitioning of ionic contrast agent via micro–computed tomography; *MFx*, microfracture.

The left glenoids underwent surgery, whereas the right glenoids served as unoperated controls. For each time point, the *P* values reflect comparisons of the operated limbs across the 3 treatment groups.

* Significantly ($P < .05$) greater than contralateral limb.

($P = .28$), or volume ($P = .11$) were detected among the surgical groups (Table I). However, relative to the injured glenoids, the contralateral unoperated joints exhibited significantly higher tissue thickness in both the UD and AMIC groups, significantly larger volume within the UD group, and significantly lower attenuation in the MFx and AMIC groups. The mean repair tissue volume ratios were 0.35 ± 0.10 for the UD group, 0.91 ± 0.43 for MFx, and 0.68 ± 0.28 for AMIC ($P = .11$).

### Histologic investigation

The total ICRS II scores (mean ± SD) for the UD, MFx, and AMIC groups were 460 ± 85, 767 ± 302, and 527 ± 244, respectively ($P = .52$). All groups showed minimal inflammation and vascular responses with no abnormal calcification. Surgical control specimens exhibited minimal repair tissue formation. In 3 of the 4 MFx samples, immature yet hyaline-like cartilage was evident from safranin O staining of proteoglycans and moderate restoration of collagen birefringence. AMIC samples exhibited primarily fibrous tissue formation with less zonal organization than was evident in the MFx group.

## 32-Week healing

### Magnetic resonance imaging

Representative T2 and T1ρ maps of intact and repaired cartilage tissue after MFx and AMIC are shown in Figure 5. The AMIC group exhibited higher T2 values relative to the MFx group (22.9 ± 1.4 milliseconds vs 19.3 ± 0.5 milliseconds, $P = .01$), whereas T1ρ was lower for the AMIC group (53.0 ± 4.0 milliseconds vs 59.6 ± 3.7 milliseconds, $P = .06$). The MFx repair tissue showed lower T2 values ($P = .043$) and higher T1ρ values ($P = .043$) compared with the contralateral control glenoids (Table II).

For both the T2 and T1ρ indexes, the ratio was closer to 1 for the AMIC group in comparison with the MFx group; specifically, the T2 index was significantly lower for the MFx group, whereas the T1ρ index was significantly higher for the MFx group ($P = .01$). The mean repair tissue volume ratios for the groups were 0.14 ± 0.14 for the UD group, 0.81 ± 0.37 for MFx, and 0.69 ± 0.20 for AMIC. The UD volume ratio ($P = .01$) was significantly lower than that of the MFx group.

For the unoperated glenoids of both the MFx and AMIC groups, the T2 of the superficial cartilage layer exceeded ($P < .01$) that of the deep layer, whereas no statistical differences in T2 were observed by depth for either the MFx ($P = .19$) or AMIC ($P = .7$) group. Conversely, for the unoperated glenoids of the MFx and AMIC treatment groups, T1ρ was similar ($P > .6$) for the superficial and deep regions, but T1ρ of the superficial layer of the repair tissue was higher ($P < .04$) than that of the deep layer in both groups (Table II).

### EPIC-μCT

The repair tissue volume was significantly ($P = .007$) higher for MFx relative to UD (Table I). Neither thickness nor attenuation varied by treatment group ($P \geq .13$). Attenuation was significantly ($P \leq .04$) higher for operated joints in comparison with contralateral glenoids in each experimental group. The contralateral glenoids exhibited greater thickness than the operated glenoids in both the UD ($P = .02$) and MFx ($P = .03$) groups, as well as increased volume in the UD ($P = .01$) and AMIC ($P = .047$) groups. The mean repair tissue volume ratios (treatment/control) were 0.42 ± 0.45 for the UD group, 0.75 ± 0.43 for MFx, and 0.84 ± 0.54 for AMIC ($P = .17$). No differences in the

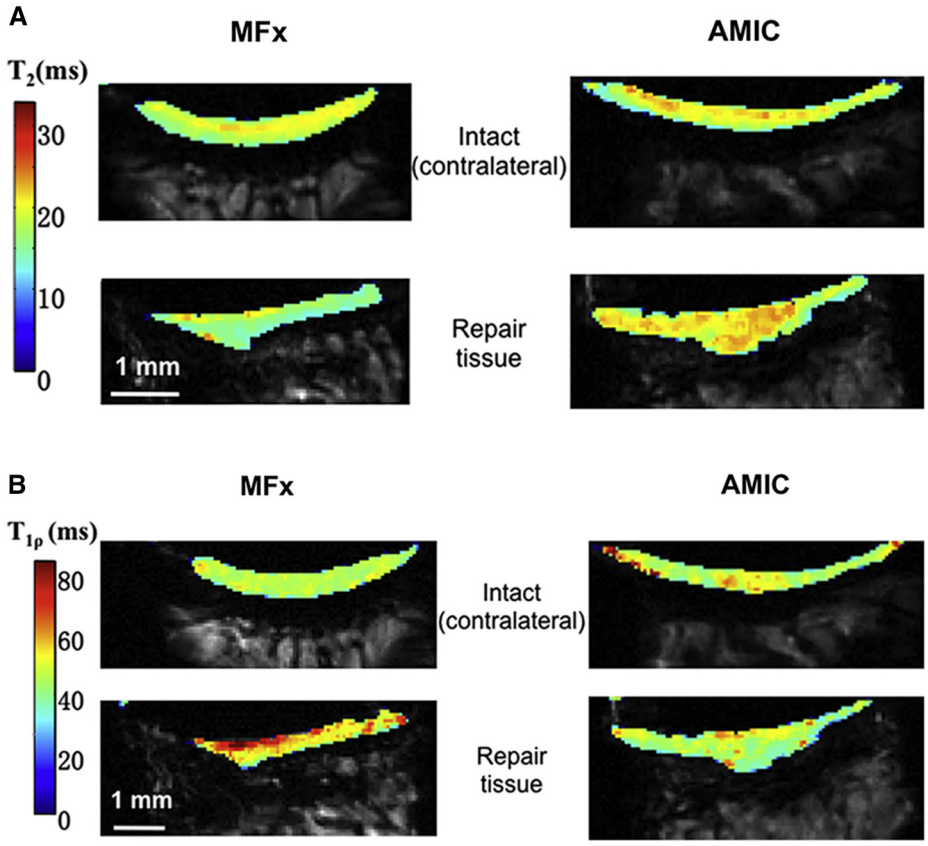


**Figure 5** Representative (**A**) T2 maps and (**B**) T1ρ maps for microfracture (MFx) and autologous matrix-induced chondrogenesis (AMIC) groups.

**Table II** High-field MRI results for MFx and AMIC groups

| | T2: full thickness, ms | T1ρ: full thickness, ms | T2: superficial, ms | T2: deep, ms | T1ρ: superficial, ms | T1ρ: deep, ms |
|---|---|---|---|---|---|---|
| MFx | | | | | | |
| Left | 19.3 ± 0.5 | 59.6 ± 3.7 | 20.7 ± 0.2 | 20.0 ± 0.8 | 62.2 ± 6.1* | 52.7 ± 3.4 |
| Right | 23.0 ± 0.8 | 51.2 ± 1.9 | 24.3 ± 0.7* | 21.0 ± 1.3 | 51.5 ± 1.8 | 51.0 ± 2.7 |
| AMIC | | | | | | |
| Left | 22.9 ± 1.4 | 53.0 ± 4.0 | 21.6 ± 0.7 | 21.3 ± 1.3 | 52.4 ± 4.9* | 49.8 ± 3.5 |
| Right | 23.7 ± 1.3 | 51.7 ± 1.8 | 24.8 ± 2.0* | 21.7 ± 2.2 | 50.1 ± 3.7 | 50.5 ± 5.1 |
| *P* value | .01 | .06 | .04 | .25 | .06 | .31 |

*AMIC*, autologous matrix-induced chondrogenesis; *MFx*, microfracture; *MRI*, magnetic resonance imaging.
Minimal repair tissue formation in the untreated defect group precluded the reliable calculation of outcomes for this group. The left glenoids underwent surgery, whereas the right glenoids served as unoperated controls. The *P* values reflect comparisons of the operated limbs between the 2 treatment groups.
* Significantly ($P < .05$) greater in superficial layer than deep layer.

volume ratio were observed at 32 weeks relative to 8 weeks after injury ($P > .6$ for all groups).

## Histologic investigation

Representative histologic images are provided in Figure 6. Total ICRS II scores were similar ($P = .28$) among the UD, MFx, and AMIC groups (676 ± 140, 716 ± 173, and 592 ± 51, respectively). For the UD group, 32-week scores showed a significant ($P = .03$) increase relative to those of the 8-week group, primarily attributable to fewer chondrocyte clusters and improved basal integration with subchondral bone. No improvements were observed with time for rabbits treated with either MFx ($P = .71$) or AMIC ($P = .32$). Qualitatively, the results indicated inferior healing in the AMIC and UD groups relative to the MFx group, for

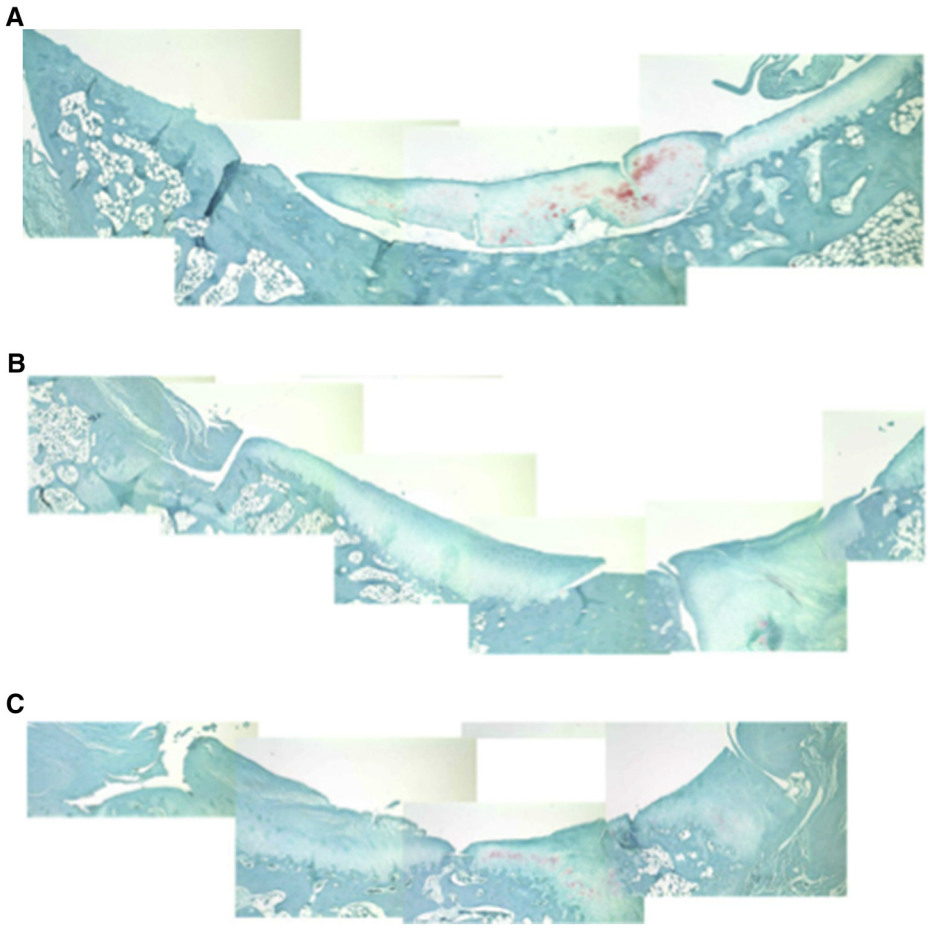


**Figure 6** Safranin O–stained histologic images of representative samples from each treatment group at 32 weeks after injury. (**A**) In the untreated defect group, fibrous repair tissue was evident, with poor integration with subchondral bone. (**B**) In the microfracture group, a robust fibrous tissue response was observed, with the structural organization of the matrix similar to that of normal cartilage. (**C**) In the autologous matrix-induced chondrogenesis group, a variable amount of fibrous repair tissue was observed along the joint, with sparse presence of chondrocytes. (Original magnification x16.)

which basal integration and tidemark formation improved over time whereas overall cartilage structure did not.

## Discussion

Although treatment of glenohumeral arthrosis with arthroplasty or hemiarthroplasty is highly effective in patients of advanced age,[26] a younger, more active population of patients requires alternative strategies to preserve the joint in addition to improving symptoms and function.[10] Regarding alternatives to arthroplasty, the glenoid remains particularly challenging to manage in relatively young patients.[37] Although there have been several reports indicating that MFx provides symptomatic pain relief of glenohumeral arthritis,[12,36] very little is known regarding tissue-level responses to such treatments. Therefore, in this study, we developed a novel rabbit model of glenoid chondral injury to investigate the intrinsic healing potential of glenoid cartilage as well as repair responses after MFx alone or MFx with collagen scaffold. Our research group has extensive experience with the rabbit GHJ for investigating cartilage responses to anesthetic agents,[13,19,20] and in the present study, we sought to adapt this animal model for in vivo studies of healing of surgically created articular defects. The rabbit appears to be a clinically relevant in vivo model for glenohumeral cartilage repair because, in contrast to other large animal models (eg, sheep, horse, dog) whose forelimbs are continuously under load, the rabbit shows increased reliance on its hind legs for weight bearing and frequently unloads its forelimbs (and thus the GHJ) while at rest.

Although EPIC-μCT and histologic results of the early repair response (8 weeks) appeared to support the premise that healing was least effective in the UD group, few statistically significant outcomes were observed in this regard (Table I). The mean ratios of tissue volume of the repair to the contralateral glenoid were 0.35 ± 0.10, 0.91 ± 0.43, and 0.68 ± 0.28 for the UD, MFx, and AMIC groups, respectively, but this comparison did not reach significance

($P = .11$), likely attributable to one perceived MFx outlier whose volume ratio was 0.35. Comparisons between contralateral shoulders within each group, however, showed that repair tissue in the UD group had lower ($P = .01$) thickness and volume than the intact glenoid. The volume ratio did not improve with time for any of the groups. Histologic analyses indicated that improvements over time were only evident regarding basal integration of repair tissue with the subchondral bone (UD and MFX groups), as well as with development of the tidemark (MFx group); no improvements in overall cartilage structure or cellular features were noted for any of the treatment groups.

MRI mapping of the T1ρ and T2 relaxation times is increasingly being used as a noninvasive tool to supplement clinical assessment of articular cartilage injuries of the knee, hip, and ankle.[5,15,24,44,50] In our study, at 32 weeks after injury, high-field MRI showed a lower ($P = .01$) T1ρ index (ie, ratio of T1ρ of repair tissue to that of contralateral intact joint) for the AMIC group relative to the MFx group. As T1ρ exhibits a linear, negative correlation with proteoglycan content,[1,8] increased T1ρ values in MFx-treated glenoids relative to contralateral intact cartilage indicate repair tissue with decreased proteoglycan content. Meanwhile, the lower T2 index of the MFx group ($P = .01$) indicates a higher fibrous tissue composition with lower free water content relative to AMIC treatment. These results are consistent with longer-term follow-up studies (eg, >2 years postoperatively) in humans that reported that repair tissue after MFx exhibits lower T2 values[52,53] and higher T1ρ values[50] relative to regions of normal cartilage. Repair tissue volume (expressed as a percentage of the contralateral glenoid) was similar for the AMIC and MFx groups ($P = .8$), each of which exhibited a higher volume ratio than the untreated controls ($P = .03$ and $P = .01$, respectively). Furthermore, the T2 and T1ρ indexes for the AMIC group were closer to 1.0 than was observed in the MFX group, which indicates that AMIC treatment may promote regeneration of extracellular matrix more closely resembling that of the native joint. Analysis of T2 and T1ρ through the tissue depth provides further insight into the microstructural organization of the repair tissue in our model. Whereas T2 decreased significantly with depth in the unoperated glenoid cartilage (consistent with prior reports[31,50]), no regional variation was observed in MFx- and AMIC-treated tissues (Table II), implying a lack of organization in the regenerated fibrous matrix at 8 months after injury.

Whereas our T1ρ results suggest that the proteoglycan content of AMIC repair tissue (in comparison with MFx) was more similar to that of normal hyaline cartilage, interestingly, this observation was not confirmed with μCT or histologic investigation. The lack of consistent results between μCT and MRI assays may be attributable to the considerably smaller voxels available for the former. Of note, 32-week histologic results were obtained from a separate group of rabbits from those analyzed for MRI and μCT (Fig. 1), and although the same surgeon performed all of the procedures, it is possible that healing responses differed among animals within the separate treatment group.

Several characterizations of cartilage healing with a type I/III collagen matrix have shown cellular architecture that more closely resembles that of native tissue.[3,46] Sheep articular chondrocytes grown on a type I/III collagen scaffold adhered firmly to the scaffold and exhibited a chondrocyte-like morphology.[9] Type I/III collagen matrices used with the AMIC procedure in animals and in retrospective clinical studies have indicated promising results.[16,18,30] However, to our knowledge, no prior studies have assessed AMIC treatment for glenohumeral chondral injury. Given that MRI outcomes represented the only significantly improved metrics of healing conferred by AMIC, the results of our investigation do not strongly support the use of a bilayer collagen patch to augment the glenoid chondral healing response elicited by MFx treatment alone. A potential reason for this is that patch durability may not be adequate to stabilize the healing clot within the entire glenoid surface, particularly because the glenoid experiences a high duty cycle of loading attributable to its small surface area relative to that of the humeral head. In contrast, the beneficial effects of MFx were observed with both μCT (repair tissue thickness and volume at 8 and 32 weeks, respectively) and histologic investigation (evidence of hyaline-like cartilage features at both time points), although significant differences were noted in comparison with the UD group only.

In contrast to widely used models of focal defects (eg, in rabbit knees), our model uses a complete removal of the glenoid articular surface; this is clinically relevant to the ''ream and run'' technique, which helps to preserve joint space (likely via deposition of fibrocartilage) and improve function clinically.[7,32] Unlike the method in our study, in which the glenoid articular surface was reamed to the calcified layer, Matsen et al[34] assessed healing following reaming of the glenoid into the subchondral and bleeding cancellous bone after performing hemiarthroplasty in canines. At 10 weeks after injury, granulation tissue partially replaced the reamed surface, and a robust fibrocartilaginous tissue repair response was observed at 24 weeks. Lee et al[29] regenerated the entire articular surface and subchondral bone in rabbits in which the native humeral head was excised at the metaphyseal junction. Four months after injury, in their UD group, chondrocytes were scarcely observed amidst fibrous tissue in the synovial space. The results of our study suggesting limited intrinsic healing capacity of the rabbit glenoid cartilage are therefore similar to those of the canine glenoid and rabbit humeral head investigations.

Limitations of this study include the variability of results within each treatment group, which—though not uncommon for in vivo animal studies—may have contributed to the lack of significant differences in μCT

and histologic results. Furthermore, the surgical approach to the GHJ required transection and repair of the supraspinatus and infraspinatus tendons. These tendon defects likely induced a localized inflammatory environment in the initial postoperative period, although the effect of this concurrent healing process on glenoid chondral healing is unknown.

## Conclusion

The purpose of this study was to develop a novel rabbit model of glenoid cartilage healing that is amenable to detailed, quantitative investigation of repair tissue structure and composition using clinically relevant surgical approaches. Neither MFx nor AMIC uniformly enhanced the amount or quality of repair tissue relative to untreated glenoid chondral defects. However, improvements conferred by AMIC were limited to MRI outcomes, whereas MFx appeared to promote increased fibrous tissue deposition via μCT and more hyaline-like repair histologically. Therefore, the results from this study suggest that the addition of a MFx procedure promotes biologic resurfacing of the glenoid. Future studies examining strategies to further augment the efficacy of MFx treatment are needed to improve our understanding of the healing process.

## Acknowledgments

The authors gratefully acknowledge funding received through a Junior Investigator Grant (V.M.W.) from the Musculoskeletal Transplant Foundation as well as National Institutes of Health grants EB007537 (R.L.M.) and AR052272 (D.R.S.). Micro–computed tomography imaging and analyses were conducted using the Rush MicroCT/Histology Core. The technical assistance of Lev Rappoport, MD, and Elizabeth Shewman, MS, is gratefully acknowledged.

## Disclaimer

Geoffrey S. Van Thiel, Susan Chubinskaya, Nikhil N. Verma, Anthony A. Romeo, and Brian J. Cole report that they have received financial remuneration (including research support from for-profit entities) for work related to the subject of this article.

The other authors, their immediate families, and any research foundations with which they are affiliated have not received any financial payments or other benefits from any commercial entity related to the subject of this article.

## References

1. Akella SV, Regatte RR, Gougoutas AJ, Borthakur A, Shapiro EM, Kneeland JB, et al. Proteoglycan-induced changes in T1rho-relaxation of articular cartilage at 4T. Magn Reson Med 2001;46:419-23.
2. Benthien JP, Behrens P. The treatment of chondral and osteochondral defects of the knee with autologous matrix-induced chondrogenesis (AMIC): method description and recent developments. Knee Surg Sports Traumatol Arthrosc 2011;19:1316-9. http://dx.doi.org/10.1007/s00167-010-1356-1
3. Buma P, Pieper JS, van Tienen T, van Susante JL, van der Kraan PM, Veerkamp JH, et al. Cross-linked type I and type II collagenous matrices for the repair of full-thickness articular cartilage defects—a study in rabbits. Biomaterials 2003;24:3255-63. http://dx.doi.org/10.1016/S0142-9612(03)00143-1
4. Bydder M, Rahal A, Fullerton GD, Bydder GM. The magic angle effect: a source of artifact, determinant of image contrast, and technique for imaging. J Magn Reson Imaging 2007;25:290-300. http://dx.doi.org/10.1002/jmri.20850
5. Carballido-Gamio J, Joseph GB, Lynch JA, Link TM, Majumdar S. Longitudinal analysis of MRI T2 knee cartilage laminar organization in a subset of patients from the osteoarthritis initiative: a texture approach. Magn Reson Med 2011;65:1184-94. http://dx.doi.org/10.1002/mrm.22693
6. Chu CR, Szczodry M, Bruno S. Animal models for cartilage regeneration and repair. Tissue Eng Part B Rev 2010;16:105-15. http://dx.doi.org/10.1089/ten.TEB.2009.0452
7. Clinton J, Franta AK, Lenters TR, Mounce D, Matsen FA III. Nonprosthetic glenoid arthroplasty with humeral hemiarthroplasty and total shoulder arthroplasty yield similar self-assessed outcomes in the management of comparable patients with glenohumeral arthritis. J Shoulder Elbow Surg 2007;16:534-8. http://dx.doi.org/10.1016/j.jse.2006.11.003
8. Duvvuri U, Goldberg AD, Kranz JK, Hoang L, Reddy R, Wehrli FW, et al. Water magnetic relaxation dispersion in biological systems: the contribution of proton exchange and implications for the noninvasive detection of cartilage degradation. Proc Natl Acad Sci U S A 2001;98:12479-84.
9. Ehlers EM, Fuss M, Rohwedel J, Russlies M, Kuhnel W, Behrens P. Development of a biocomposite to fill out articular cartilage lesions. Light, scanning and transmission electron microscopy of sheep chondrocytes cultured on a collagen I/III sponge. Ann Anat 1999;181:513-8.
10. Elser F, Braun S, Dewing CB, Millett PJ. Glenohumeral joint preservation: current options for managing articular cartilage lesions in young, active patients. Arthroscopy 2010;26:685-96. http://dx.doi.org/10.1016/j.arthro.2009.10.017
11. Erggelet C, Endres M, Neumann K, Morawietz L, Ringe J, Haberstroh K, et al. Formation of cartilage repair tissue in articular cartilage defects pretreated with microfracture and covered with cell-free polymer-based implants. J Orthop Res 2009;27:1353-60. http://dx.doi.org/10.1002/jor.20879
12. Frank RM, Van Thiel GS, Slabaugh MA, Romeo AA, Cole BJ, Verma NN. Clinical outcomes after microfracture of the glenohumeral joint. Am J Sports Med 2010;38:772-81. http://dx.doi.org/10.1177/0363546509350304
13. Friel NA, McNickle AG, DeFranco MJ, Wang FC, Shewman EF, Verma NN, et al. The effect of highly purified capsaicin on articular cartilage and rotator cuff tendon healing: an in vivo rabbit study. Trans Orthop Res Soc 2010;abstract:1166. http://www.ors.org/abstract-search/.
14. Fuss M, Ehlers EM, Russlies M, Rohwedel J, Behrens P. Characteristics of human chondrocytes, osteoblasts and fibroblasts seeded onto a type I/III collagen sponge under different culture conditions. A light, scanning and transmission electron microscopy study. Ann Anat 2000;182:303-10.

15. Giannini S, Buda R, Battaglia M, Cavallo M, Ruffilli A, Ramponi L, et al. One-step repair in talar osteochondral lesions: 4-year clinical results and t2-mapping capability in outcome prediction. Am J Sports Med 2013;41:511-8. http://dx.doi.org/10.1177/0363546512467622
16. Gille J, Behrens P, Volpi P, de Girolamo L, Reiss E, Zoch W, et al. Outcome of autologous matrix induced chondrogenesis (AMIC) in cartilage knee surgery: data of the AMIC Registry. Arch Orthop Trauma Surg 2013;133:87-93. http://dx.doi.org/10.1007/s00402-012-1621-5
17. Gille J, Kunow J, Boisch L, Behrens P, Bos I, Hoffmann C, et al. Cell-laden and cell-free matrix-induced chondrogenesis versus microfracture for the treatment of articular cartilage defects: a histological and biomechanical study in sheep. Cartilage 2010;1:29-42. http://dx.doi.org/10.1177/1947603509358721
18. Gille J, Schuseil E, Wimmer J, Gellissen J, Schulz AP, Behrens P. Mid-term results of autologous matrix-induced chondrogenesis for treatment of focal cartilage defects in the knee. Knee Surg Sports Traumatol Arthrosc 2010;18:1456-64. http://dx.doi.org/10.1007/s00167-010-1042-3
19. Gomoll AH, Kang RW, Williams JM, Bach BR, Cole BJ. Chondrolysis after continuous intra-articular bupivacaine infusion: an experimental model investigating chondrotoxicity in the rabbit shoulder. Arthroscopy 2006;22:813-9, http://dx.doi.org/10.1016/j.arthro.2006.06.006
20. Gomoll AH, Yanke AB, Kang RW, Chubinskaya S, Williams JM, Bach BR, et al. Long-term effects of bupivacaine on cartilage in a rabbit shoulder model. Am J Sports Med 2009;37:72-7. http://dx.doi.org/10.1177/0363546508323748
21. Grumet RC, Hadley S, Diltz MV, Lee TQ, Gupta R. Development of a new model for rotator cuff pathology: the rabbit subscapularis muscle. Acta Orthop 2009;80:97-103. http://dx.doi.org/10.1080/17453670902807425
22. Hammond LC, Lin EC, Harwood DP, Juhan TW, Gochanour E, Klosterman EL, et al. Clinical outcomes of hemiarthroplasty and biological resurfacing in patients aged younger than 50 years. J Shoulder Elbow Surg 2013;22:1345-51. http://dx.doi.org/10.1016/j.jse.2013.04.015
23. Hildebrand T, Rüegsegger P. A new method for the model-independent assessment of thickness in three-dimensional images. J Microsc 1997;185:67-75.
24. Holtzman DJ, Theologis AA, Carballido-Gamio J, Majumdar S, Li X, Benjamin C. T(1rho) and T(2) quantitative magnetic resonance imaging analysis of cartilage regeneration following microfracture and mosaicplasty cartilage resurfacing procedures. J Magn Reson Imaging 2010;32:914-23. http://dx.doi.org/10.1002/jmri.22300
25. Hsu EW, Schoeniger JS, Bowtell R, Aiken NR, Horsman A, Blackband SJ. A modified imaging sequence for accurate T2 measurements using NMR microscopy. J Magn Reson B 1995;109:66-9.
26. Jain N, Pietrobon R, Hocker S, Guller U, Shankar A, Higgins LD. The relationship between surgeon and hospital volume and outcomes for shoulder arthroplasty. J Bone Joint Surg Am 2004;86:496-505.
27. Karabork H. Three-dimensional measurements of glenohumeral joint surfaces in sheep, cat and rabbit by photogrammetry. J Animal Vet Adv 2009;8:1248-51.
28. Kotwal N, Li J, Sandy J, Plaas A, Sumner DR. Initial application of EPIC-μCT to assess mouse articular cartilage morphology and composition: effects of aging and treadmill running. Osteoarthritis Cartilage 2012;20:887-95. http://dx.doi.org/10.1016/j.joca.2012.04.012
29. Lee CH, Cook JL, Mendelson A, Moioli EK, Yao H, Mao JJ. Regeneration of the articular surface of the rabbit synovial joint by cell homing: a proof of concept study. Lancet 2010;376:440-8. http://dx.doi.org/10.1016/S0140-6736(10)60668-X
30. Lee YH, Suzer F, Thermann H. Autologous matrix-induced chondrogenesis in the knee: a review. Cartilage 2014;5:145-53. http://dx.doi.org/10.1177/1947603514529445
31. Li X, Pai A, Blumenkrantz G, Carballido-Gamio J, Link T, Ma B, et al. Spatial distribution and relationship of T1rho and T2 relaxation times in knee cartilage with osteoarthritis. Magn Reson Med 2009;61:1310-8. http://dx.doi.org/10.1002/mrm.21877
32. Lynch JR, Franta AK, Montgomery WH Jr, Lenters TR, Mounce D, Matsen FA III. Self-assessed outcome at two to four years after shoulder hemiarthroplasty with concentric glenoid reaming. J Bone Joint Surg Am 2007;89:1284-92. http://dx.doi.org/10.2106/JBJS.E.00942
33. Mainil-Varlet P, Van Damme B, Nesic D, Knutsen G, Kandel R, Roberts S. A new histology scoring system for the assessment of the quality of human cartilage repair: ICRS II. Am J Sports Med 2010;38:880-90. http://dx.doi.org/10.1177/0363546509359068
34. Matsen FA III, Clark JM, Titelman RM, Gibbs KM, Boorman RS, Deffenbaugh D, et al. Healing of reamed glenoid bone articulating with a metal humeral hemiarthroplasty: a canine model. J Orthop Res 2005;23:18-26. http://dx.doi.org/10.1016/j.orthres.2004.06.019
35. Menezes NM, Gray ML, Hartke JR, Burstein D. T2 and T1ρ MRI in articular cartilage systems. Magn Reson Med 2004;51:503-9. http://dx.doi.org/10.1002/mrm.10710
36. Millett PJ, Huffard BH, Horan MP, Hawkins RJ, Steadman JR. Outcomes of full-thickness articular cartilage injuries of the shoulder treated with microfracture. Arthroscopy 2009;25:856-63. http://dx.doi.org/10.1016/j.arthro.2009.02.009
37. Nicholson GP, Goldstein JL, Romeo AA, Cole BJ, Hayden JK, Twigg SL, et al. Lateral meniscus allograft biologic glenoid arthroplasty in total shoulder arthroplasty for young shoulders with degenerative joint disease. J Shoulder Elbow Surg 2007;16(Suppl):S261-6. http://dx.doi.org/10.1016/j.jse.2007.03.003
38. Nieminen MT, Rieppo J, Toyras J, Hakumaki JM, Silvennoinen J, Hyttinen MM, et al. T2 relaxation reveals spatial collagen architecture in articular cartilage: a comparative quantitative MRI and polarized light microscopic study. Magn Reson Med 2001;46:487-93.
39. Othman SF, Li J, Abdullah O, Moinnes JJ, Magin RL, Muehleman C. High-resolution/high-contrast MRI of human articular cartilage lesions. Acta Orthop 2007;78:536-46.
40. Palmer AW, Guldberg RE, Levenston ME. Analysis of cartilage matrix fixed charge density and three-dimensional morphology via contrast-enhanced microcomputed tomography. Proc Natl Acad Sci U S A 2006;103:19255-60. http://dx.doi.org/10.1073/pnas.0606406103
41. Parsons IM IV, Millett PJ, Warner JJ. Glenoid wear after shoulder hemiarthroplasty: quantitative radiographic analysis. Clin Orthop Relat Res 2004;421:120-5.
42. Peptan IA, Hong L, Xu H, Magin RL. MR assessment of osteogenic differentiation in tissue-engineered constructs. Tissue Eng 2006;12:843-51. http://dx.doi.org/10.1089/ten.2006.12.843
43. Potter HG, Foo LF. Magnetic resonance imaging of articular cartilage: trauma, degeneration, and repair. Am J Sports Med 2006;34:661-7. http://dx.doi.org/10.1177/0363546505281938
44. Rakhra KS, Lattanzio PJ, Cardenas-Blanco A, Cameron IG, Beaule PE. Can T1-rho MRI detect acetabular cartilage degeneration in femoroacetabular impingement?: A pilot study. J Bone Joint Surg Br 2012;94:1187-92. http://dx.doi.org/10.1302/0301-620X.94B9.29981
45. Salzmann GM, Paul J, Bauer JS, Woertler K, Sauerschnig M, Landwehr S, et al. T2 assessment and clinical outcome following autologous matrix-assisted chondrocyte and osteochondral autograft transplantation. Osteoarthritis Cartilage 2009;17:1576-82. http://dx.doi.org/10.1016/j.joca.2009.07.010
46. Schlegel W, Nurnberger S, Hombauer M, Albrecht C, Vecsei V, Marlovits S. Scaffold-dependent differentiation of human articular chondrocytes. Int J Mol Med 2008;22:691-9. http://dx.doi.org/10.3892/ijmm_00000074
47. Sperling JW, Cofield RH, Rowland CM. Minimum fifteen-year follow-up of Neer hemiarthroplasty and total shoulder arthroplasty in patients aged fifty years or younger. J Shoulder Elbow Surg 2004;13:604-13. http://dx.doi.org/10.1016/j.jse.2004.03.013

48. Steadman JR, Rodkey WG, Rodrigo JJ. Microfracture: surgical technique and rehabilitation to treat chondral defects. Clin Orthop Relat Res 2001;391:S362-9.
49. Strauss EJ, Verma NN, Salata MJ, McGill KC, Klifto C, Nicholson GP, et al. The high failure rate of biologic resurfacing of the glenoid in young patients with glenohumeral arthritis. J Shoulder Elbow Surg 2014;23: 409-19. http://dx.doi.org/10.1016/j.jse.2013.06.001
50. Theologis AA, Schairer WW, Carballido-Gamio J, Majumdar S, Li X, Ma CB. Longitudinal analysis of T1ρ and T2 quantitative MRI of knee cartilage laminar organization following microfracture surgery. Knee 2012;19:652-7. http://dx.doi.org/10.1016/j.knee.2011.09.004
51. Wegener B, Schrimpf FM, Pietschmann MF, Milz S, Berger-Lohr M, Bergschmidt P, et al. Matrix-guided cartilage regeneration in chondral defects. Biotechnol Appl Biochem 2009;53(Pt 1):63-70. http://dx.doi.org/10.1042/BA20080020
52. Welsch GH, Mamisch TC, Domayer SE, Dorotka R, Kutscha-Lissberg F, Marlovits S, et al. Cartilage T2 assessment at 3-T MR imaging: in vivo differentiation of normal hyaline cartilage from reparative tissue after two cartilage repair procedures—initial experience. Radiology 2008;247:154-61. http://dx.doi.org/10.1148/radiol.2471070688
53. Welsch GH, Trattnig S, Domayer S, Marlovits S, White LM, Mamisch TC. Multimodal approach in the use of clinical scoring, morphological MRI and biochemical T2-mapping and diffusion-weighted imaging in their ability to assess differences between cartilage repair tissue after microfracture therapy and matrix-associated autologous chondrocyte transplantation: a pilot study. Osteoarthritis Cartilage 2009; 17:1219-27. http://dx.doi.org/10.1016/j.joca.2009.03.018
54. Wingerd BD. Rabbit dissection manual. Baltimore: Johns Hopkins University Press; 1985.
55. Xie L, Lin AS, Guldberg RE, Levenston ME. Nondestructive assessment of sGAG content and distribution in normal and degraded rat articular cartilage via EPIC-microCT. Osteoarthritis Cartilage 2010; 18:65-72. http://dx.doi.org/10.1016/j.joca.2009.07.014
56. Xie L, Lin AS, Levenston ME, Guldberg RE. Quantitative assessment of articular cartilage morphology via EPIC-microCT. Osteoarthritis Cartilage 2009;17:313-20. http://dx.doi.org/10.1016/j.joca.2008.07.015